Acta Geotechnica (2006, Vol. 1, No. 1, pp. 59-73)

Experimental evidence of a unique flow rule of non-cohesive soils under high-cyclic loading

T. Wichtmann*, A. Niemunis, Th. Triantafyllidis

Institute of Soil Mechanics and Foundation Engineering, Ruhr-University Bochum, Universitätsstraße 150, 44801 Bochum, Germany

Abstract

The presented results of cyclic triaxial tests on sand demonstrate that the cumulative effects due to small cycles obey a kind of flow rule. It mainly depends on the average stress ratio about which the cycles are performed. This so-called "cyclic flow rule" is unique and can be well approximated by flow rules for monotonic loading. Amongst others it is shown that the cyclic flow rule is only moderately influenced by the average mean pressure, by the strain loop (span, shape, polarization), the void ratio, the loading frequency, the static preloading and the grain size distribution curve. A slight increase of the compactive portion of the flow rule with increasing residual strain (due to the previous cycles) was observed. These experimental findings prove that the cyclic flow rule is an essential and indispensable concept in explicit (N-type) accumulation models.

Key words: Cyclic flow rule; Direction of strain accumulation; Cyclic triaxial tests; Sand

1 Introduction

Cyclic loading leads to an accumulation (of stress or strain) in soils. This paper deals with high-cyclic loading ($N \geq 10^4$) with relatively small amplitudes ($\varepsilon^{\text{ampl}} < 10^{-3}$). In FE predictions of residual settlements two numerical strategies can be distinguished, the *implicit* and the *explicit* one. In the implicit method each cycle is calculated with a $\dot{\boldsymbol{\sigma}}$-$\dot{\boldsymbol{\varepsilon}}$ constitutive model (e.g. with an elastoplastic multi-surface model, e.g. [11], an endochronic model, e.g. [20] or the hypoplastic model with intergranular strain [5, 8, 14, 21]) and many strain increments. Due to the unintentional accumulation of systematic (e.g. numerical) errors [12] and the huge calculation effort [22], the application of this method is restricted to a low number of cycles (say, $N < 50$).

For high-cyclic loading explicit models are more suitable. Several such models were proposed in the literature [1,3,4,6,7,10,15–18]. They treat the accumulation of residual strain or stress under cyclic loading similar to the problem of creep under constant loads. The basic constitutive equation is similar to that of viscoplastic models with the number of cycles N replacing time t:

$$\dot{\boldsymbol{\sigma}} = \mathsf{E} : (\dot{\boldsymbol{\varepsilon}} - \dot{\boldsymbol{\varepsilon}}^{\text{acc}}) \tag{1}$$

with the Jaumann stress rate $\dot{\boldsymbol{\sigma}}$ of the Cauchy stress $\boldsymbol{\sigma}$, the stretching $\dot{\boldsymbol{\varepsilon}}$ (in our case obtained as the material derivative of the Hencky's logarithmic strain $\boldsymbol{\varepsilon}$, but with positive compression), the given accumulation rate $\dot{\boldsymbol{\varepsilon}}^{\text{acc}}$ and the pressure-dependent elastic stiffness E. In the context of cyclic loading "rate" means a derivative with respect to the number of cycles N (instead of time t), i.e. $\dot{\sqcup} = \partial \sqcup / \partial N$. Explicit models predict the average accumulation curve without following the strain path during the particular cycles. The given accumulation rate $\dot{\boldsymbol{\varepsilon}}^{\text{acc}}$ can be written as a product of a scalar intensity of strain accumulation $\dot{\varepsilon}^{\text{acc}}$ and a tensorial direction of strain accumulation (cyclic flow rule $\mathbf{m}$ = unit tensor):

$$\dot{\boldsymbol{\varepsilon}}^{\text{acc}} \quad = \quad \dot{\varepsilon}^{\text{acc}}\, \mathbf{m} \tag{2}$$

The following sections present the results of numerous drained cyclic triaxial tests in order to examine the variability and to establish an empirical formula for $\mathbf{m}(\boldsymbol{\sigma}^{\text{av}}, ...)$. The influence of the average stress, of the stress loop (span, shape, polarization), the void ratio, the loading frequency, the static preloading and

*Corresponding author. Tel.: + 49-234-3226080; fax: +49-234-3214150; *e-mail address:* torsten.wichtmann@rub.de

the grain size distribution curve is studied. It is demonstrated that $\mathbf{m}$ depends essentially on the average stress ratio $\eta^{\mathrm{av}} = q^{\mathrm{av}}/p^{\mathrm{av}}$. This dependence can be well approximated by the flow rules of constitutive models for monotonic loading (e.g. modified Cam clay model, hypoplastic model).

These experimental findings facilitate the development of explicit accumulation models. The flow rule $\mathbf{m}$ can be treated separately from the intensity $\dot{\varepsilon}^{\mathrm{acc}}$. Regrettably, only few models [1, 15, 18] incorporate such kind of flow rule.

2 Notation

The sign convention of soil mechanics (compression positive) is used. The notation is given for the triaxial test with the axial stress σ_1 and the lateral stress $\sigma_2 = \sigma_3$. The Roscoe invariants p (mean pressure) and q (deviatoric stress) of the Cauchy stress $\boldsymbol{\sigma}$ are

$$p = \frac{1}{3}(\sigma_1 + 2\,\sigma_3) \tag{3}$$

$$q = \sigma_1 - \sigma_3 \tag{4}$$

Alternatively, the isomorphic variables $P = \sqrt{3}\,p$ and $Q = \sqrt{2/3}\,q$ may be used [13]. The obliquity of stress in the p-q-plane (Fig. 1) is described by the stress ratio $\eta = q/p$. The inclinations of the critical state line (CSL, from monotonic tests) and the failure line in the p-q-plane (Fig. 1) are $M_c = (6\,\sin\varphi)/(3 - \sin\varphi)$ for compression and $M_e = -(6\,\sin\varphi)/(3 + \sin\varphi)$ for extension with the critical friction angle $\varphi = \varphi_c$ for the CSL and the peak friction angle $\varphi = \varphi_p$ for the maximum shear strength.

Figure 1 shows a typical stress path of a cyclic triaxial test in the p-q-plane. An average stress $\boldsymbol{\sigma}^{\mathrm{av}}$ is superposed by a cyclic portion. An oscillation of the axial stress $\sigma_1(t)$ and the lateral stress $\sigma_3(t)$ without a time shift results in *in-phase* stress cycles with a certain inclination $\tan\alpha = q^{\mathrm{ampl}}/p^{\mathrm{ampl}}$ in the p-q-plane (Fig. 1). For the special case $\sigma_3 = \mathrm{const.}$ ($\tan\alpha = 3$) the amplitude ratio $\zeta = q^{\mathrm{ampl}}/p^{\mathrm{av}}$ is used. If $\sigma_1(t)$ and $\sigma_3(t)$ are applied with a time shift more complex stress paths (e.g. ellipses in the p-q-plane, *out-of-phase*-cycles) can be tested.

The axial strain is denoted by ε_1 and the lateral one by $\varepsilon_2 = \varepsilon_3$. The strain invariants (ε_v = volumetric strain, ε_q = deviatoric strain) are

$$\varepsilon_v = \varepsilon_1 + 2\,\varepsilon_3 \tag{5}$$

$$\varepsilon_q = \frac{2}{3}\,(\varepsilon_1 - \varepsilon_3) \tag{6}$$

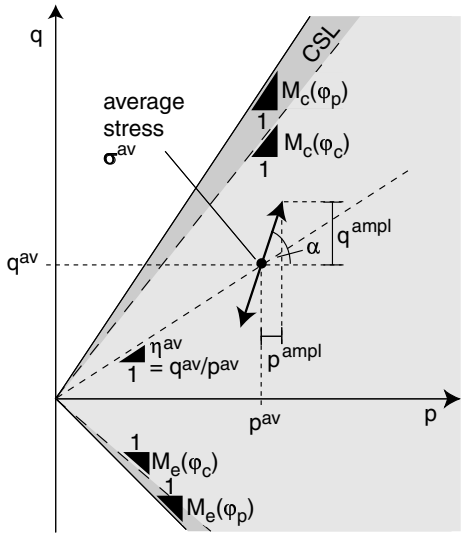

Figure 1: *Cyclic stress path in the p-q-plane*

Their rates are work-conjugated to the Roscoe invariants p and q. The axial strain is calculated from $\varepsilon_1 = \ln(h_0/h)$ and the volumetric one from $\varepsilon_v = \ln(V_0/V)$ with the initial height h_0 of the sample, the actual height h, the initial volume V_0 and the actual volume V. The isomorphic strain invariants are $\varepsilon_P = 1/\sqrt{3}\,\varepsilon_v$ and $\varepsilon_Q = \sqrt{3/2}\,\varepsilon_q$. The total strain is

$$\varepsilon = \sqrt{(\varepsilon_1)^2 + 2(\varepsilon_3)^2} = \sqrt{(\varepsilon_P)^2 + (\varepsilon_Q)^2} \tag{7}$$

In the case of cyclic loading the strain $\boldsymbol{\varepsilon}$ is composed of an accumulated (residual) portion ($\boldsymbol{\varepsilon}^{\mathrm{acc}}$) and an elastic (resilient) portion ($\boldsymbol{\varepsilon}^{\mathrm{ampl}}$) as shown in Fig. 2. The ratios

$$\Omega = \frac{\dot{\varepsilon}_v^{\mathrm{acc}}}{\dot{\varepsilon}_q^{\mathrm{acc}}} \quad \text{and} \quad \omega = \frac{\varepsilon_v^{\mathrm{acc}}}{\varepsilon_q^{\mathrm{acc}}} \tag{8}$$

are used as scalar measures of the flow rule $\mathbf{m}$. The density is described by the index $I_D = (e_{\max} - e)/(e_{\max} - e_{\min})$ with void ratio e. The initial value after consolidation prior to cyclic loading is denoted by I_{D0}.

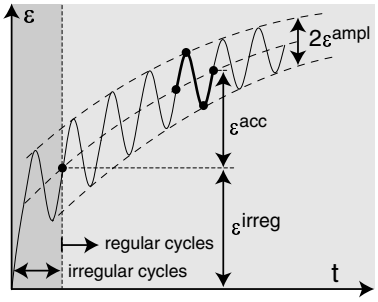

Figure 2: *Development of strain in a cyclic triaxial test*

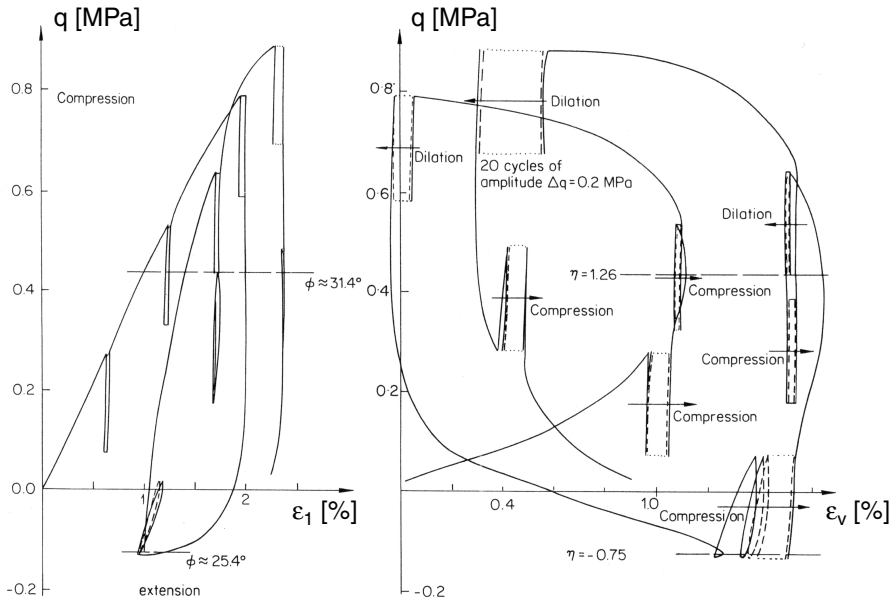

Figure 3: *Contractive or dilative soil behaviour under cyclic loading in dependence on q^{av} after Luong [9]: a) q-ε_1-loops, b) q-ε_v-loops*

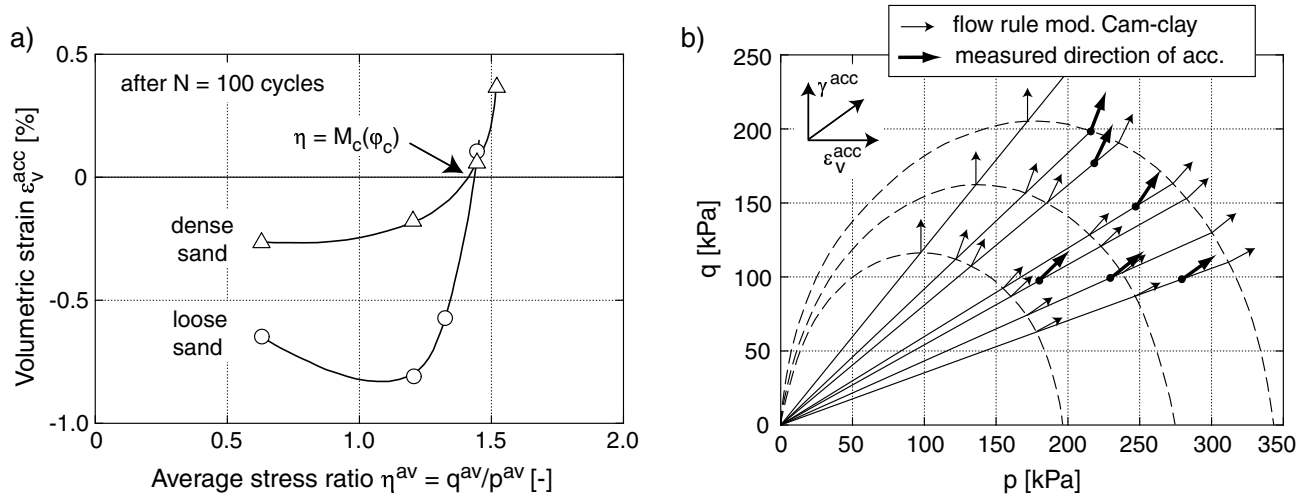

Figure 4: *Studies on the direction of strain accumulation after Chang & Whitman [2]: a) residual volumetric strains ε_v^{acc} after 100 cycles as a function of the average stress ratio η^{av}, b) measured directions of strain accumulation in the p-q-plane compared to the flow rule of the modified Cam clay model*

3 Literature survey

There are few studies on the direction of strain accumulation under cyclic loading and those publications mostly deal with a low number of cycles. In a drained cyclic triaxial test Luong [9] applied packages of 20 cycles each at different average deviatoric stresses q^{av}. The right part of Fig. 3 shows the measured q-ε_v-loops. For low values of q^{av} the material behaviour was contractive while it was dilative at larger q^{av}. Luong defined a so-called "characteristic threshold (CT) line" in the p-q-plane separating the contractive ($\boldsymbol{\sigma}^{av}$ below CT line) from the dilative ($\boldsymbol{\sigma}^{av}$ above CT line) material behaviour. This (border)line was found independent of the soil density.

Another important observation on the direction of strain accumulation was made by Chang & Whitman [2]. In a series of cyclic triaxial tests on medium coarse to coarse sand the average mean pressure p^{av} was constant while the stress ratio η^{av} was varied from test to test. Four tests were performed on loose and four other ones on dense specimens. In Fig. 4a the residual volumetric strain after 100 cycles is shown as a function

of η^{av}. Independently of the sand density, $\dot{\varepsilon}_v^{\mathrm{acc}} = 0$ was observed for $\eta^{\mathrm{av}} \approx M_c(\varphi_c)$. Thus, Chang & Whitman [2] assumed the CT-line of Luong [9] to be identical with the critical state line (CSL). For $\eta^{\mathrm{av}} < M_c(\varphi_c)$ a densification and for $\eta^{\mathrm{av}} > M_c(\varphi_c)$ a dilative material behaviour was measured.

In other tests Chang & Whitman [2] observed that the ratio $\gamma^{\mathrm{acc}}/\varepsilon_v^{\mathrm{acc}}$ with $\gamma = \varepsilon_1 - \varepsilon_3 = 3/2\varepsilon_q$ increased with η^{av}. A good approximation of the measured direction of strain accumulation by the flow rule of the modified Cam clay model

$$\omega \quad = \quad \frac{M_c(\varphi_c)^2 - (\eta^{\mathrm{av}})^2}{2\eta^{\mathrm{av}}} \tag{9}$$

has been demonstrated for different sands (Fig. 4b). No influence of the average mean pressure p^{av} and the amplitude ratio $\zeta = q^{\mathrm{ampl}}/p^{\mathrm{av}}$ on ω could be detected. Also the influence of the number of cycles was reported negligible. However, the tests of Chang & Whitman [2] were restricted to 1,050 cycles. It is therefore not clear if the test results can be extrapolated to larger numbers of cycles. Furthermore, only the case $\sigma_3 =$ constant was tested.

The studies of Luong [9] and Chang & Whitman [2] as well as our own experiments presented within this paper are restricted to relatively *small* amplitudes. For *large* stress amplitudes with $q^{\min} \approx 0$ and $q^{\max} \approx M_c(\varphi_p)$, Suiker et al. [19] reported a dilative behaviour (during the first approx. 1,000 cycles) although the average stress (defined as $q^{\mathrm{av}} = \frac{1}{2}(q^{\max} + q^{\min})$) lay below the critical state line. In that case, the residual strain and also the flow rule $\dot{\varepsilon}_v^{\mathrm{acc}}/\dot{\varepsilon}_q^{\mathrm{acc}}$ depends on the time the stress path is resting on the failure line.

4 Test device, testing procedure and tested materials

A scheme of the used triaxial cell is given in Fig. 5. A detailed description of this test device (four of them were available in the present study) can be found in [23]. Specimens (diameter $d = 10$ cm, height $h = 20$ cm) were prepared by dry pluviation out of a funnel through air into split moulds. Afterwards the specimens were saturated with de-aired water. A back pressure of 200 kPa was used in all tests. The procedure of specimen preparation is explained more detailed in [23]. In order to minimize friction the end plates were lubricated and a thin latex membrane was applied. In the analysis of the tests the deformation of this membrane (bedding error) was carefully subtracted from the deformation of the soil skeleton.

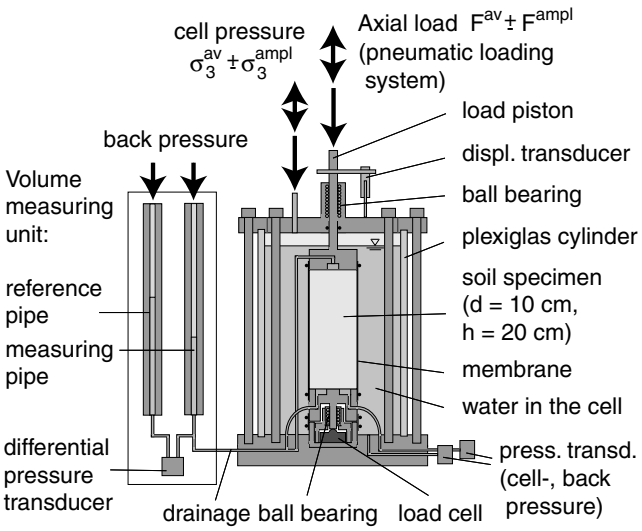

Figure 5: *Scheme of triaxial cell*

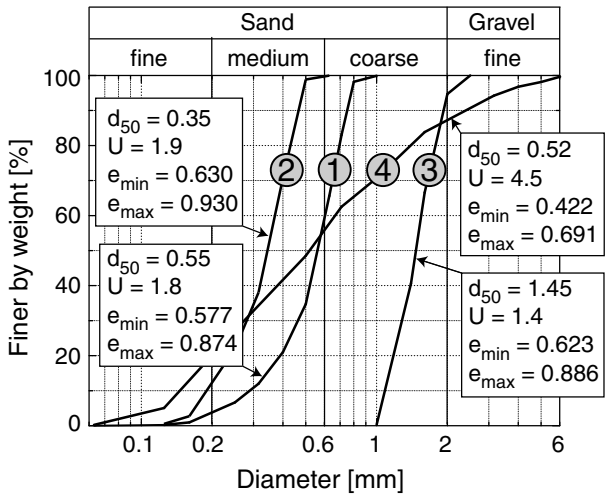

Figure 6: *Tested grain size distributions*

The axial load was applied by a pneumatic loading system and was measured inside the pressure cell (Fig. 5). The axial deformation of the specimen was measured by means of a displacement transducer which was attached to the load piston. The volume changes were determined via the pore water. For this purpose a differential pressure transducer was employed. Also the cell pressure and the back pressure were measured. During cyclic loading the signals of all transducers were recorded by means of a data acquisition system. In order to reduce the amount of data five complete cycles were sampled in certain intervals. The distance between these recordings was increased logarithmically with the number of cycles N.

Specimens were consolidated for one hour under the average effective stress $\boldsymbol{\sigma}^{\mathrm{av}}$. After that resting period σ_1 and σ_3 were cyclically varied. Since usually large

deformations occur during the first, so-called *irregular* cycle (see Fig. 2) in order to prevent an unintentional pore-pressure build-up, a low frequency of $f_B = 0.01$ Hz was used during this cycle. Afterwards usually 10^5 cycles were applied with a loading frequency $f_B = 1$ Hz.

The tests were performed on a quartz sand with subangular grain shape. The four tested grain size distribution curves are presented in Fig. 6. Most of the tests were performed on the medium to coarse sand No. 1.

5 Test results

5.1 Influence of the average stress

Numerous tests were performed with in-phase stress cycles (σ_3 = constant) at different average stresses $\boldsymbol{\sigma}^{\mathrm{av}}$. The average mean pressure (50 kPa $\leq p^{\mathrm{av}} \leq$ 300 kPa) and the average stress ratio $-0.88 \leq \eta^{\mathrm{av}} \leq 1.375$ were varied from test to test. The tested average stresses cover the cases of triaxial compression ($\eta^{\mathrm{av}} > 0$) as well as triaxial extension ($\eta^{\mathrm{av}} < 0$). In Fig. 7 they are illustrated in the p-q-plane. The specimens were prepared with similar initial densities ($0.57 \leq I_{D0} \leq 0.69$). In the tests with $\eta^{\mathrm{av}} > 0$ amplitude ratios $\zeta = q^{\mathrm{ampl}}/p^{\mathrm{av}} = 0.3$ were tested. In the tests with triaxial extension a smaller ratio $\zeta = 0.2$ was chosen due to the smaller distance of $\boldsymbol{\sigma}^{\mathrm{av}}$ to the yield surface. For this reason, in the tests with η^{av} = -0,75 and η^{av} = -0,88 even amplitude ratios of $\zeta = 0.1$ and $\zeta = 0.05$, respectively, were applied.

First the tests with $p^{\mathrm{av}} = 200$ kPa are considered. In Fig. 8 for selected average stress ratios η^{av}, the residual deviatoric strain $\varepsilon_q^{\mathrm{acc}}$ in the regular cycles is plotted versus the accumulated volumetric strain $\varepsilon_v^{\mathrm{acc}}$. The data points correspond to the numbers of cycles N = 2, 5, 10, 20, 50, 100, ..., 10^5. From Fig. 8 it is apparent that the direction of strain accumulation significantly depends on the average stress ratio η^{av}. At an isotropic average stress ($\eta^{\mathrm{av}} = 0$) a pure volumetric accumulation (densification) takes place while the rate of deviatoric strain vanishes ($\dot{\varepsilon}_q^{\mathrm{acc}} = 0$). With increasing absolute value of the average stress ratio $|\eta^{\mathrm{av}}| = |q^{\mathrm{av}}/p^{\mathrm{av}}|$ the deviatoric component of the direction of strain accumulation increases in comparison to the volumetric portion. At an average stress on the (monotonic) critical state line ($\eta^{\mathrm{av}} = M_c(\varphi_c) = 1.25$ or $\eta^{\mathrm{av}} = M_e(\varphi_c) = -0.88$, respectively) only the deviatoric strain accumulates and a vanishing rate of volumetric strain ($\dot{\varepsilon}_v^{\mathrm{acc}} = 0$) could be observed (at least during the first cycles). The latter remains valid despite the material is not at the critical density. For $M_e(\varphi_c) \leq \eta^{\mathrm{av}} \leq M_c(\varphi_c)$ a densification of the sand and within the overcritical regime a dilative behaviour was

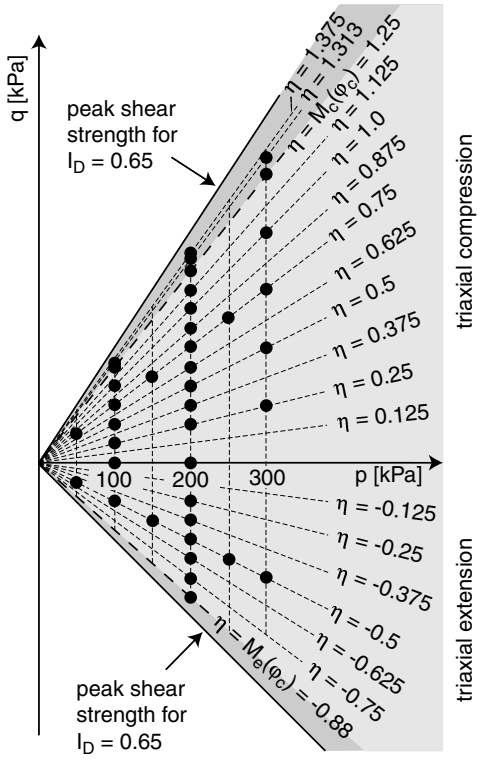

Figure 7: *Tested average stresses*

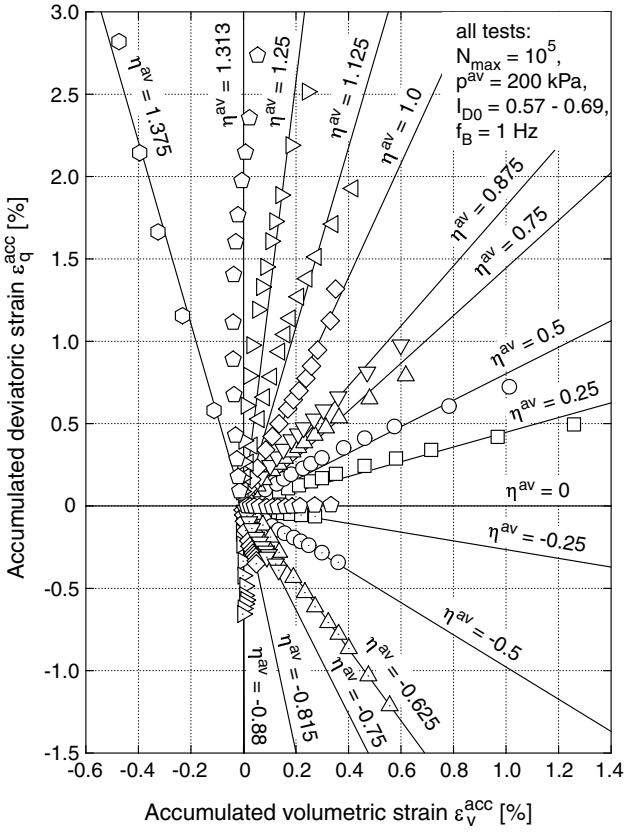

Figure 8: ε_q^{acc}-ε_v^{acc}*-strain paths for* $p^{av} = 200$ *kPa and different average stress ratios* $-0.88 \leq \eta^{av} \leq 1.375$

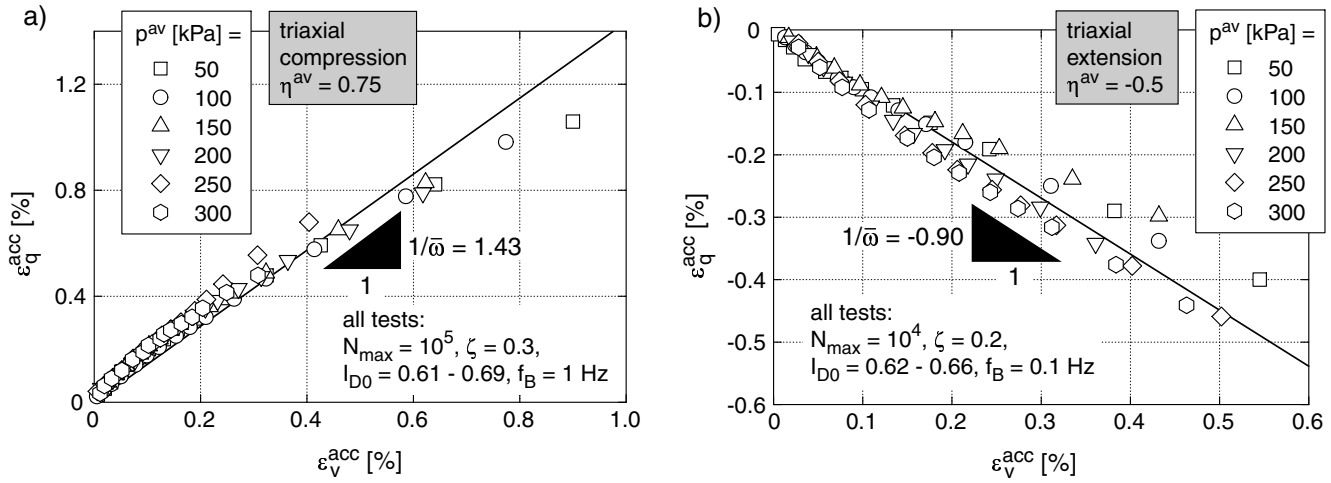

Figure 9: ε_q^{acc}-ε_v^{acc}-*strain paths for different average mean pressures: a) tests with* $\eta^{av} = 0.75$ *(triaxial compression), b) tests with* $\eta^{av} = -0.5$ *(triaxial extension)*

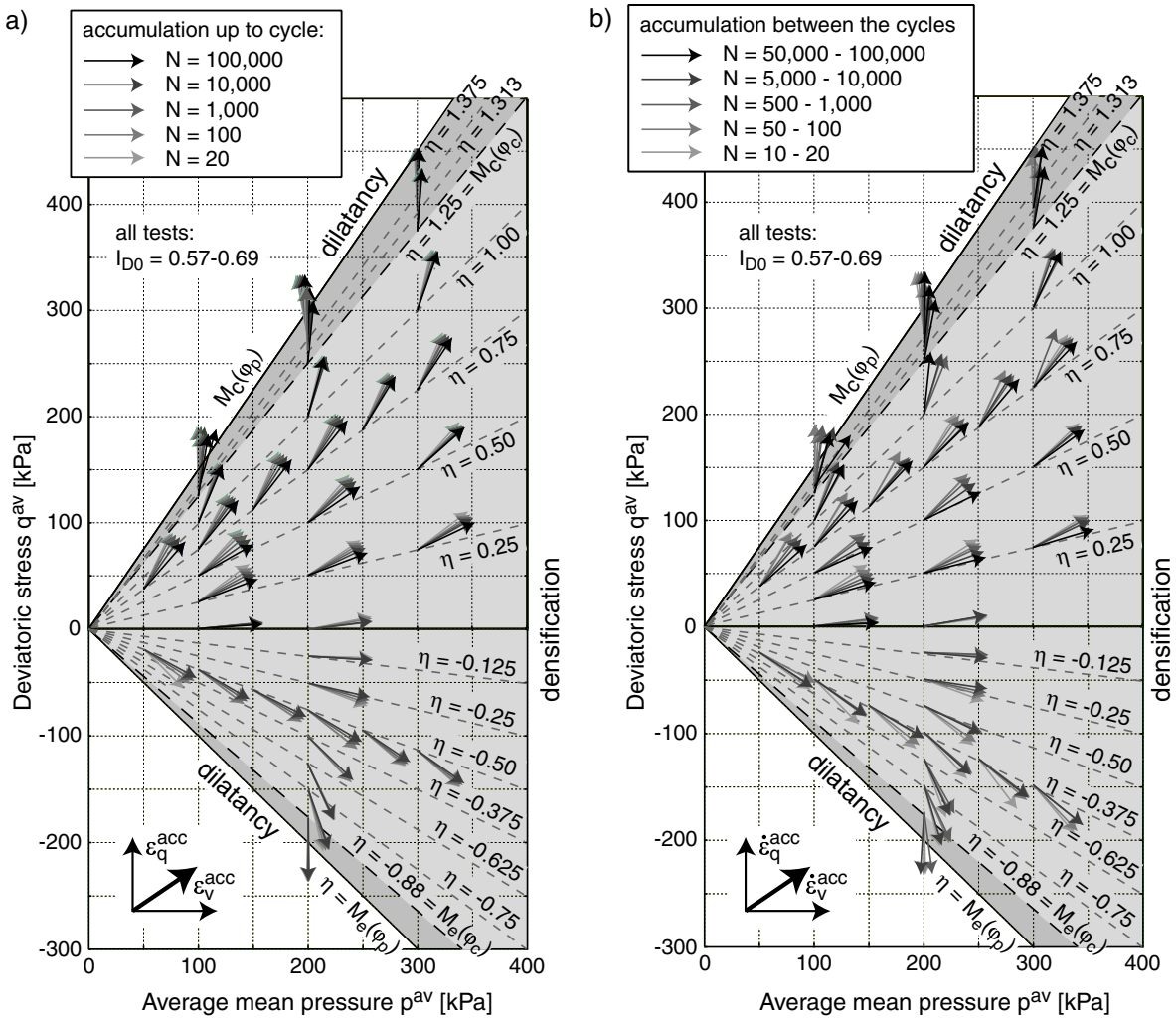

Figure 10: *Direction of strain accumulation* $\mathbf{m}$ *for different average stresses* $\boldsymbol{\sigma}^{av}$*, shown as a unit vector in the p-q-plane, a) determined from the total strain accumulated up to a certain number of cycles* N*, b) determined from the strain increments between two data recordings*

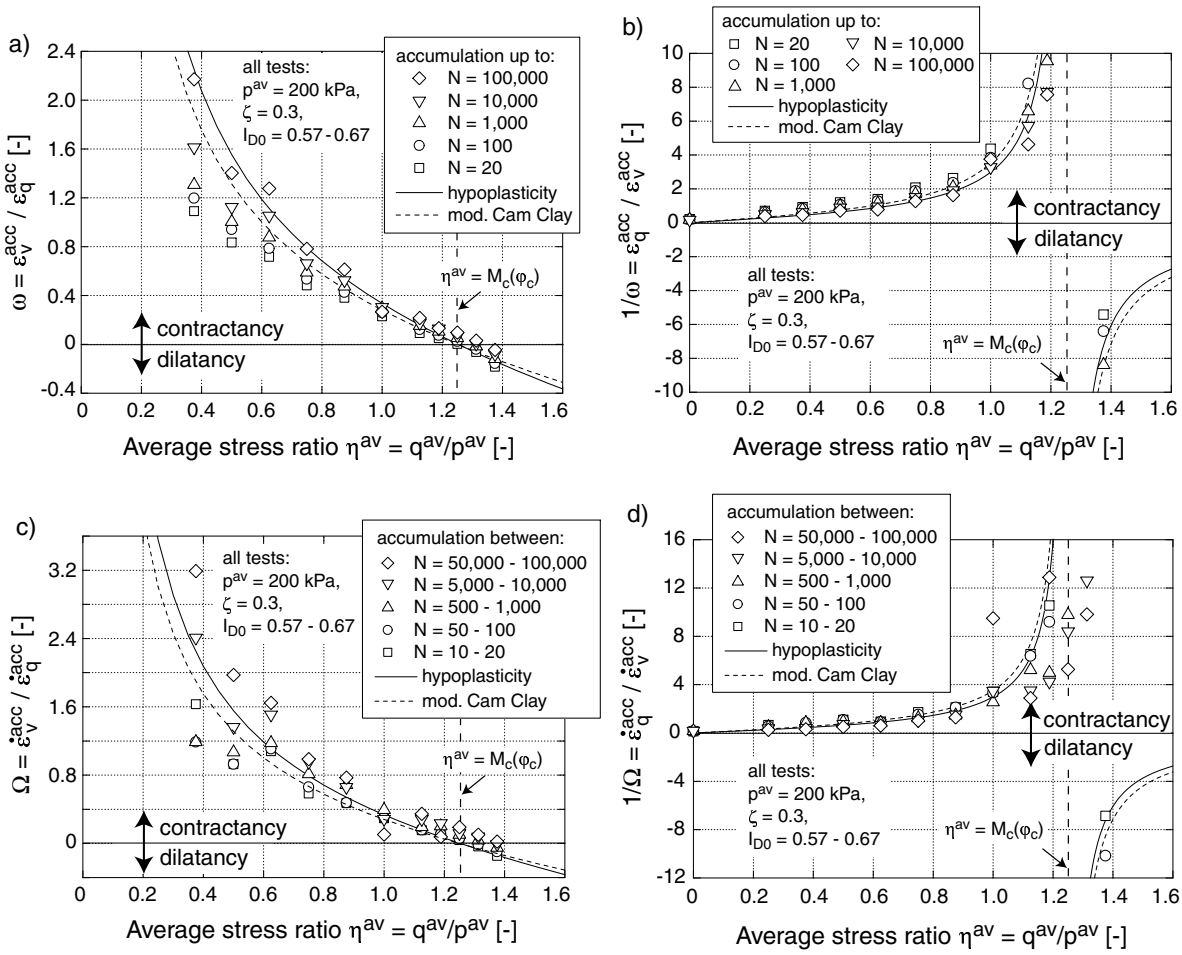

Figure 11: *Direction of strain accumulation in dependence on the stress ratio η^{av} for p^{av} = 200 kPa and triaxial compression: a) strain ratio $\omega = \varepsilon_v^{acc}/\varepsilon_q^{acc}$, b) reciprocal value $1/\omega$, c) strain ratio $\Omega = \dot{\varepsilon}_v^{acc}/\dot{\varepsilon}_q^{acc}$, d) reciprocal value $1/\Omega$*

observed (see e.g. the test with $\eta^{av} = 1.375$). The measured dependence $\mathbf{m}(\eta^{av})$ agrees well with the results of the experiments of Luong [9] and Chang & Whitman [2] (Section 3).

A slight increase of the compactive portion of the direction of strain accumulation with the number of cycles could be detected. This is depicted e.g. in Fig. 8 for the test with $\eta^{av} = M_c(\varphi_c) = 1.25$, which shows an increasing deflection of the strain path from the vertical. Similar results were obtained by Suiker et al. (2005), who measured an initial dilative and adjacent compactive behaviour for stress cycles with $\eta^{min} \approx 0$ and $\eta^{max} \approx M_c(\varphi_p)$. In our tests, the same results were obtained on dry specimens (determination of lateral strains from local measurements with non-contact displacement transducers) and on the saturated ones (measurement of volume changes via the pore water). Thus, it is unlikely that this effect is caused by measurement technique errors. Moreover, this tendency seems to be independent of the loading frequency (Section 5.5), i.e. the duration of the test. An increase of the water level in the measurement pipe, i.e. an increase of the squeezed-out water volume (see Fig. 5), due to a densification of the specimen leads to a slight increase of the back pressure in the specimen and thus to a reduction of the axial and lateral effective stresses, i.e. a reduction of p^{av} at q^{av} = constant. However, this increase of the stress ratio η^{av} should cause an opposite rotation of $\mathbf{m}$ (decrease of ω with N). Anyway, in the test with $\eta^{av} = M_c(\varphi_c) = 1.25$ the accumulation of volumetric deformation is small and the water level in the measurement pipe rarely changes its height.

The performed tests foster the observations by Chang & Whitman [2] that for a given η^{av}, the average mean pressure p^{av} does (at least in the tested range 50 kPa $\leq p^{av} \leq$ 300 kPa) hardly influence the direction of strain accumulation. This is demonstrated in Fig. 9a for the tests with $\eta^{av} = 0.75$ (triaxial compression) and in Fig. 9b for η^{av} = -0.5 (triaxial extension). The strain paths in the ε_q^{acc}-ε_v^{acc}-diagram coincide approximately

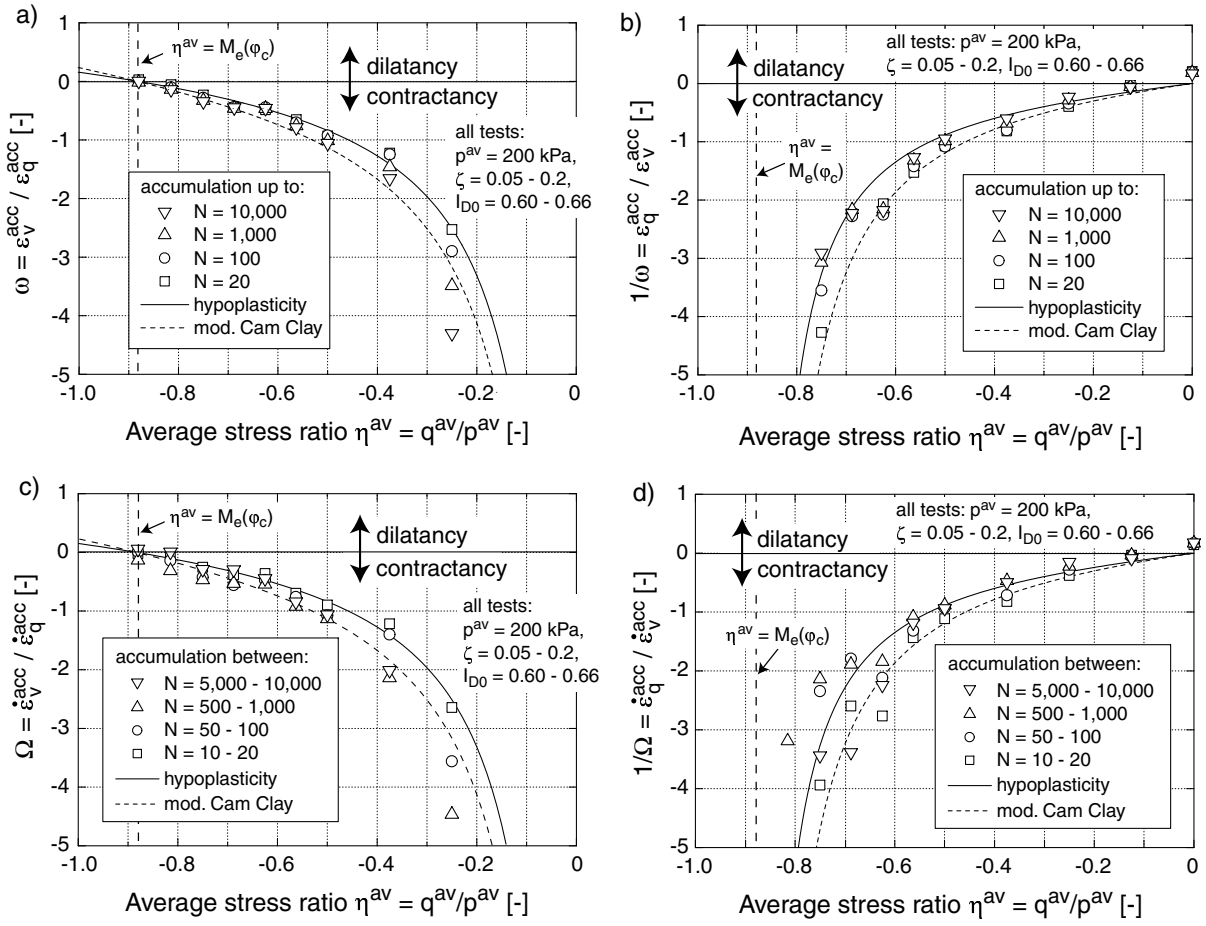

Figure 12: *Direction of strain accumulation in dependence on the stress ratio η^{av} for p^{av} = 200 kPa and triaxial extension: a) strain ratio $\omega = \varepsilon_v^{acc}/\varepsilon_q^{acc}$, b) reciprocal value $1/\omega$, c) strain ratio $\Omega = \dot{\varepsilon}_v^{acc}/\dot{\varepsilon}_q^{acc}$, d) reciprocal value $1/\Omega$*

for different average mean pressures p^{av}. From Fig. 9 it can be concluded that the increase of $\dot{\varepsilon}_v^{\mathrm{acc}}/\dot{\varepsilon}_q^{\mathrm{acc}}$ during cyclic loading is correlated with the residual strain $\varepsilon^{\mathrm{acc}}$ (due to previous cycles) rather than with N. Although all tests have been carried out up to $N = 10^5$, the smaller pressures p^{av} lead to a larger strain accumulation and hence to a larger compactive portion of $\mathbf{m}$ at equal N.

Figure 10 summarizes the measured directions of strain accumulation for all tested average stresses $\boldsymbol{\sigma}^{\mathrm{av}}$ and depicts them as unit vectors in the p-q-plane. The origin of each vector lies in (p^{av},q^{av}) of the respective test. Figure 10a was generated using the strains accumulated up to a certain number of cycles N. Thus, the inclination of the vectors to the p-axis is $1/\omega = \varepsilon_q^{\mathrm{acc}}/\varepsilon_v^{\mathrm{acc}}$. In Fig. 10b the directions of strain accumulation were calculated from the rates, i.e. the vectors are inclined by $1/\Omega = \dot{\varepsilon}_q^{\mathrm{acc}}/\dot{\varepsilon}_v^{\mathrm{acc}}$. The vectors in Fig. 10 are shown for different numbers of cycles. This is indicated by the different grayscales. The rotation of the vectors towards the positive p- or $\varepsilon_v^{\mathrm{acc}}$-axis with increasing number of cycles is of course more pronounced if shown with rates (Fig. 10b) than with the total strains (Fig. 10a).

Chang & Whitman [2] reported, that the flow rule of the modified Cam clay model, i.e. a model for monotonic loading, approximates well also the direction of strain accumulation under cyclic loading (Fig. 4b). Figure 11a shows the ratio $\omega = \varepsilon_v^{\mathrm{acc}}/\varepsilon_q^{\mathrm{acc}}$ as a function of η^{av} for the tests with $p^{\mathrm{av}} = 200$ kPa and $\eta^{\mathrm{av}} > 0$ (triaxial compression). For small stress ratios η^{av} one cannot precisely estimate ω from this diagram and therefore Fig. 11b contains a corresponding illustration of the reciprocal value $1/\omega$. Figure 11c and 11d present diagrams for the ratio of the rates $\Omega = \dot{\varepsilon}_v^{\mathrm{acc}}/\dot{\varepsilon}_q^{\mathrm{acc}}$ or its reciprocal value $1/\Omega$, respectively. The scatter is larger in the rate diagrams. Beside the measured directions of strain accumulation, also the flow rules of the modified Cam clay model (Eq. (9)) and the hypoplastic model (see e.g. Eq. (4.73) in [13]) are drawn into Fig. 11. Both flow rules (for monotonic loading) approximate well the direction of strain accumulation under cyclic loading.

Analogously to Fig. 11, Fig. 12 contains diagrams for triaxial extension ($\eta^{av} < 0$) at $p^{av} = 200$ kPa. Also for triaxial extension the modified Cam clay model and the hypoplastic model deliver a good approximation of the flow rule under cyclic loading.

5.2 Influence of the stress/strain loop (span, shape, polarization)

First in-phase stress cycles (σ_3 = constant) with p^{av} = 200 kPa and $\eta^{av} = 0.75$ (triaxial compression) are analyzed. In the tests the stress amplitude 12 kPa $\leq q^{ampl} \leq$ 80 kPa was varied. The illustration of the ε_q^{acc}-ε_v^{acc}-strain paths in Fig. 13a demonstrates, that the amplitude of the uniaxial cycles does hardly influence the cyclic flow rule. Similar tests at an average stress $p^{av} = 200$ kPa and $\eta^{av} = -0.5$ (triaxial extension, Fig. 13b) confirmed, that the ratio of the volumetric and the deviatoric accumulation rate does not significantly vary with the stress or strain amplitude.

Also the influence of the polarization of the cycles, i.e. their inclination in the stress or strain space, on **m** was studied. At $p^{av} = 200$ kPa and $\eta^{av} = 0.5$ in-phase stress cycles with six different inclinations $0° \leq \alpha_{PQ} \leq 90°$ in the P-Q-plane were tested. For each polarization four or five stress amplitudes 20 kPa $\leq \sqrt{(P^{ampl})^2 + (Q^{ampl})^2} \leq$ 100 kPa were studied. Figure 14 presents the ε_q^{acc}-ε_v^{acc}-strain paths. Each diagram contains the paths of the tests with a certain polarization α_{PQ}. Although the data shows some scatter for $\alpha_{PQ} = 10°$ and 30°, independently of the polarization α_{PQ}, the dependence of the direction of strain accumulation on the amplitude $\sqrt{(P^{ampl})^2 + (Q^{ampl})^2}$ of the cycles is small. The six diagrams in Fig. 14 provide an information about the mean value of the inclination $1/\bar{\omega}$ of the strain paths in the ε_q^{acc}-ε_v^{acc}-plane. The values lie within $0.97 \leq 1/\bar{\omega} \leq 1.27$ (i.e. 31% scatter, but the ε^{acc}-dependence of **m** has to be kept in mind). No simple correlation of $1/\bar{\omega}$ with α_{PQ} is noticeable.

Also the influence of the shape of the stress or strain cycles was tested. At $p^{av} = 200$ kPa and $\eta^{av} = 0.5$ different elliptic stress paths in the P-Q-plane were tested. Circular paths with different radii (Fig. 15a), elliptic paths with $Q^{ampl} = 80$ kPa and different spans in the direction parallel to the P-axis (Fig. 15b) as well as elliptic paths with $P^{ampl} = 80$ kPa and different amplitudes along the direction parallel to the Q-axis (Fig. 15c) were tested. The mean inclinations of the strain path in the ε_q^{acc}-ε_v^{acc}-plane (mean values of each testing series) lay within $1.15 \leq 1/\bar{\omega} \leq 1.31$, which corresponds to a scatter of 14% (considering individual pairs of tests, this scatter might be even larger). However, there seems to be no simple dependence of

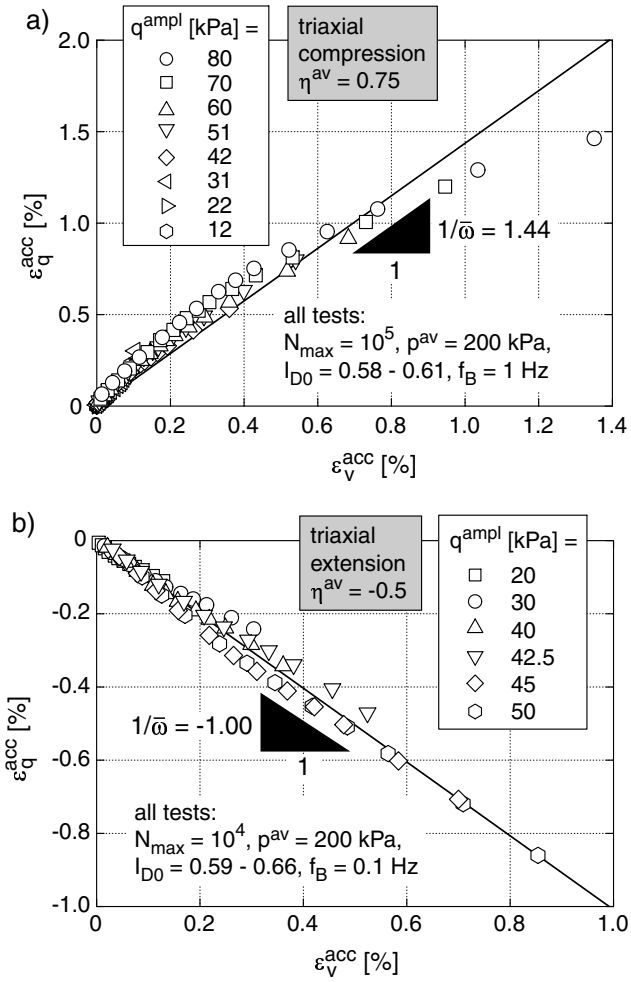

Figure 13: ε_q^{acc}-ε_v^{acc}-*strain paths for in-phase stress cycles with different amplitudes, a) tests with* $\eta^{av} = 0.75$ *(triaxial compression), b) tests with* $\eta^{av} = -0.5$ *(triaxial extension)*

the inclination $1/\bar{\omega}$ of the ε_q^{acc}-ε_v^{acc}-strain paths on the shape of the cycles.

We may thus conclude, that the influence of the size, the polarization and the shape of the stress loop (or the resulting strain loop) on **m** is not strong and may be neglected for the first in an explicit model.

5.3 Changes in the amplitude and their sequence

Figure 16 presents results of tests, in which four packages of cycles were applied in succession. Each package contained $2.5 \cdot 10^4$ cycles. At an average stress with $p^{av} = 200$ kPa and $\eta^{av} = 0.75$ the amplitudes $q^{ampl} = 20$, 40, 60 and 80 kPa were tested. The sequence of the amplitudes was varied from test to test. The strain paths in the ε_q^{acc}-ε_v^{acc}-plane are depicted in

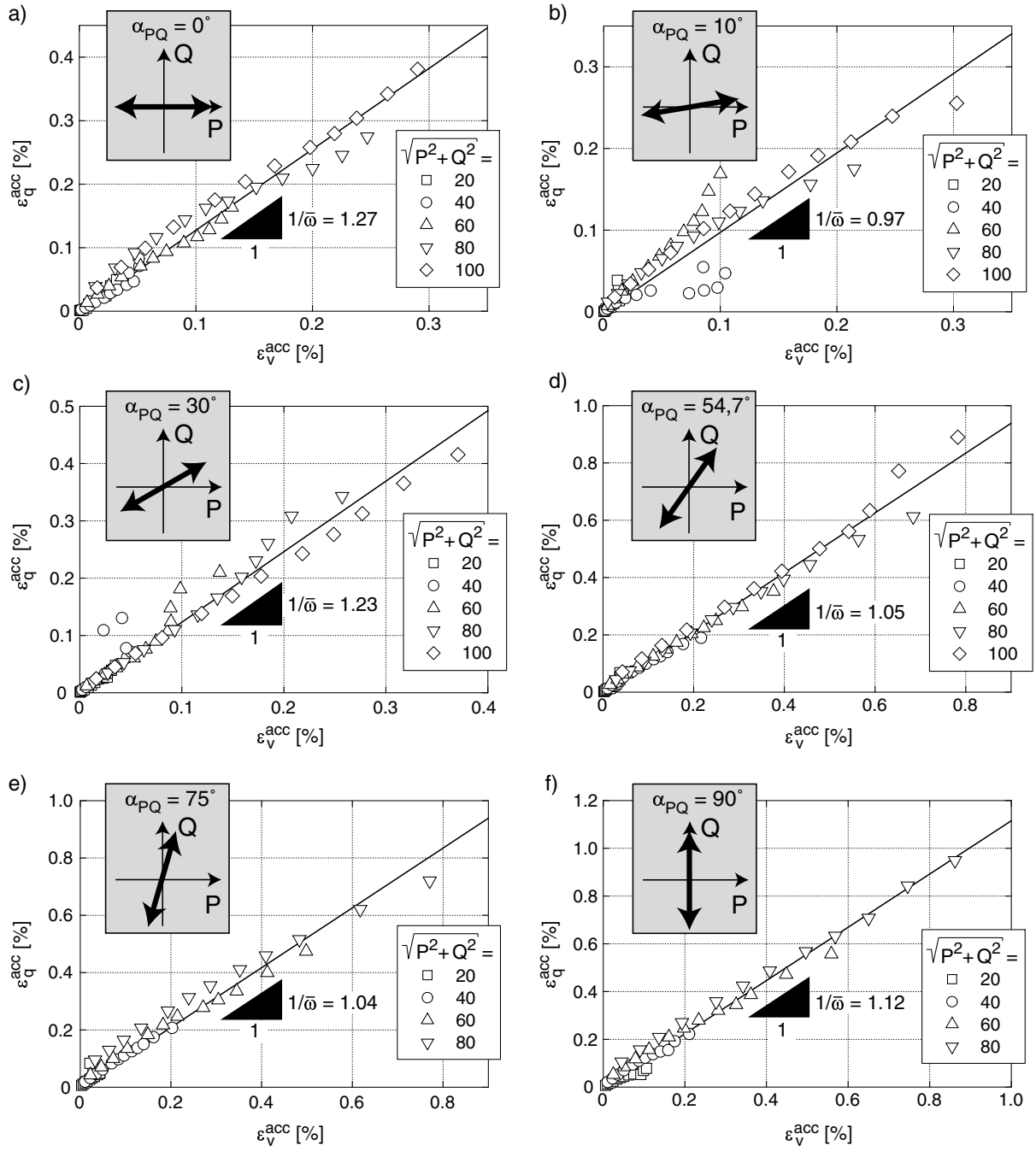

Figure 14: ε_q^{acc}-ε_v^{acc}-strain paths for in-phase stress cycles with different polarizations α_{PQ} in the P-Q-plane (all tests: $N_{\max} = 10^4$, $p^{av} = 200$ kPa, $\eta^{av} = 0.5$, $0.56 \leq I_{D0} \leq 0.64$, $f_B = 0.05$ Hz)

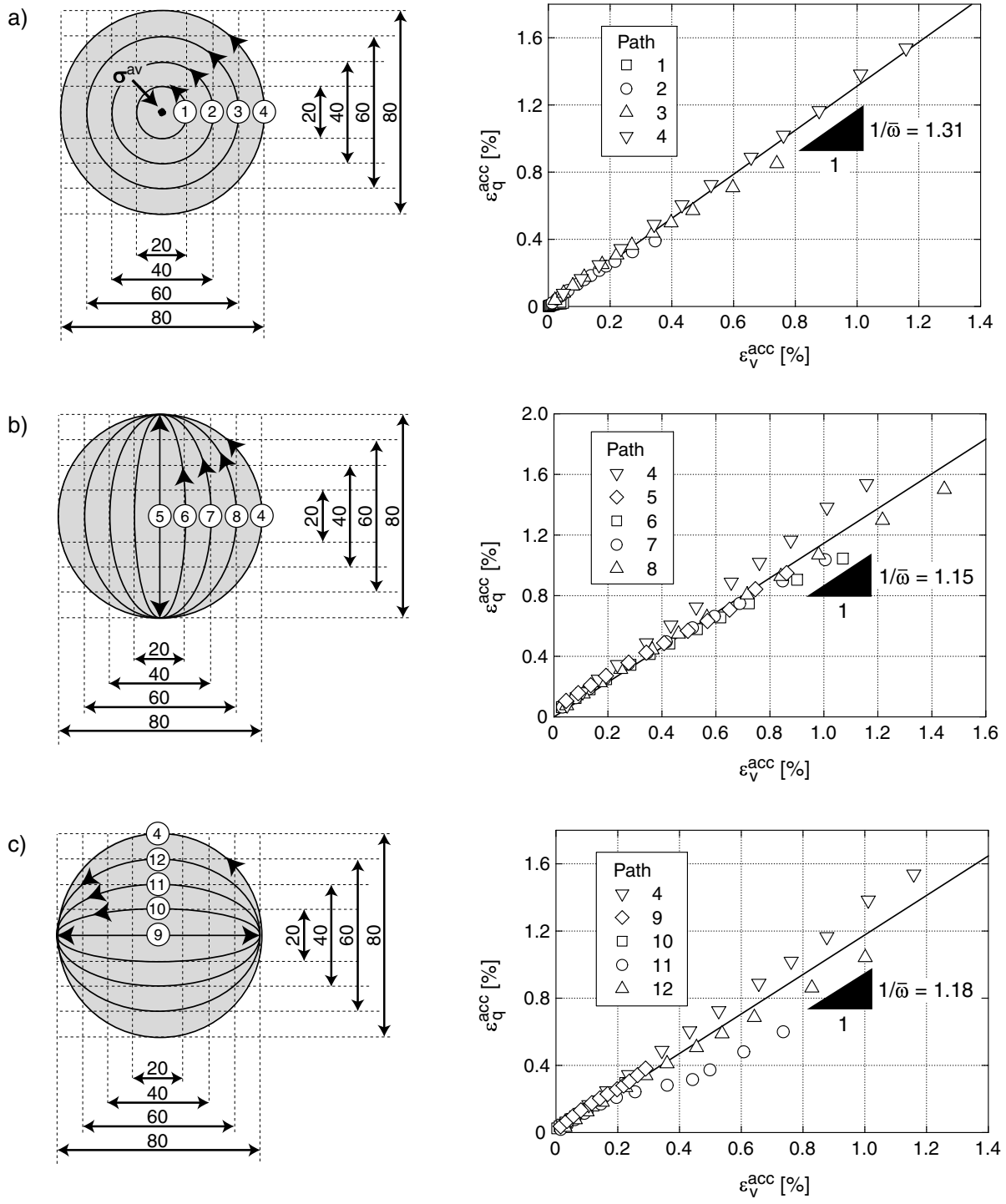

Figure 15: ε_q^{acc}-ε_v^{acc}-*strain paths for different out-of-phase (elliptic) stress paths in the P-Q-plane (all tests:* $N_{\max} = 10^4$, $p^{av} = 200$ *kPa*, $\eta^{av} = 0.5$, $0.58 \leq I_{D0} \leq 0.68$, $f_B = 0.05$ *Hz)*

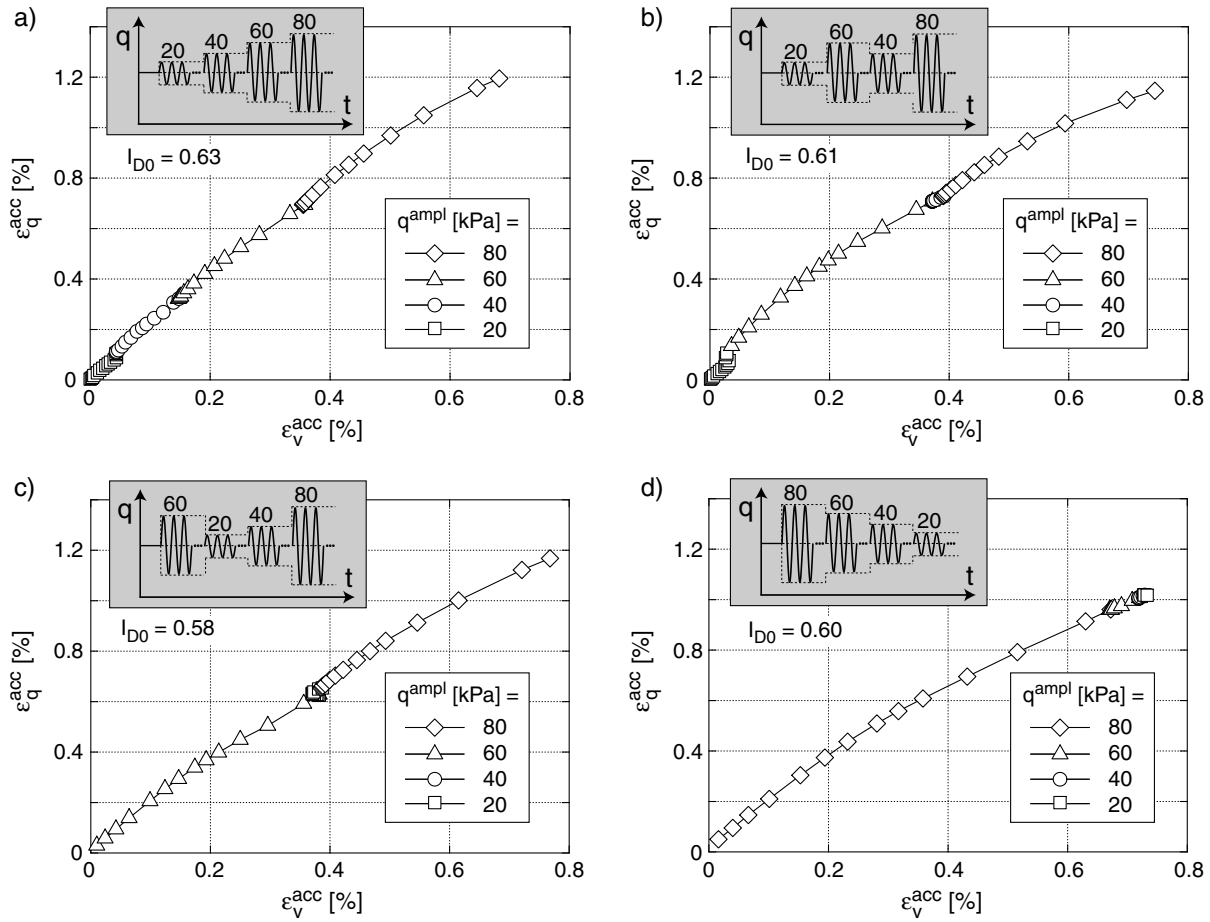

Figure 16: ε_q^{acc}-ε_v^{acc}-*strain paths in tests with four packages of cycles (all tests:* $N_{\max} = 10^5$, p^{av} *= 200 kPa,* η^{av} *= 0.75,* f_B *= 0.25 Hz)*

Fig. 16. Considering a residual volumetric strain of $\varepsilon_v^{\rm acc} = 0.7\%$, the residual deviatoric strain lies within the range $1.0\% \leq \varepsilon_q^{\rm acc} \leq 1.2\%$, i.e. the scatter is approx. 20%. A small increase of the ratio $\dot{\varepsilon}_q^{\rm acc}/\dot{\varepsilon}_v^{\rm acc}$ was measured at the beginning of a package if preceded by packages with smaller amplitudes.

5.4 Influence of the void ratio / relative density

Identical tests at different initial void ratios e_0 show similar flow directions. This is demonstrated by the strain paths in Fig. 17. The smaller inclination $1/\bar{\omega}$ in Fig. 17 in comparison to Figs. 9a and 13a can be explained by the larger residual strains in the test with $I_{D0} = 0.24$. For high initial densities ($I_{D0} > 0.9$) the values of ω scatter significantly since the ratio is calculated as the quotient of two relatively small strains. However, no clear tendency could be detected.

5.5 Influence of the loading frequency

Tests with different loading frequencies 0.05 Hz $\leq f_B \leq$ 2 Hz at identical stresses ($p^{\rm av} = 200$ kPa, $\eta^{\rm av} = 0.75$, $q^{\rm ampl} = 60$ kPa) and with similar initial densities are presented in Fig. 18. No significant influence of f_B on the cyclic flow rule could be found.

5.6 Influence of the number of cycles

The increase of the compactive portion of the direction of strain accumulation with N was discussed already in Section 5.1 for $N = 10^5$ load cycles. Figure 19 shows the results of two extremely long tests each with $2 \cdot 10^6$ cycles. The compactive portion of **m** increases also for $N > 10^5$.

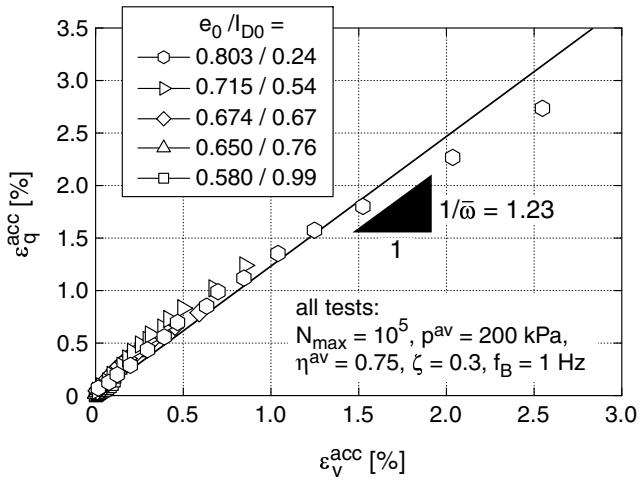

Figure 17: ε_q^{acc}-ε_v^{acc}-*strain paths in tests with different initial void ratios* e_0

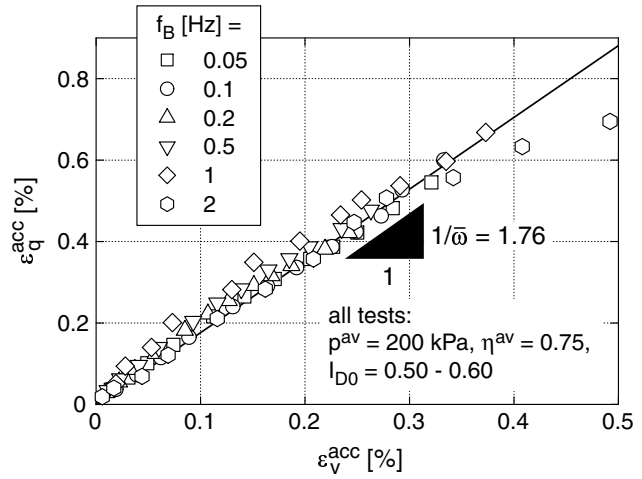

Figure 18: ε_q^{acc}-ε_v^{acc}-*strain paths in tests with different loading frequencies* f_B

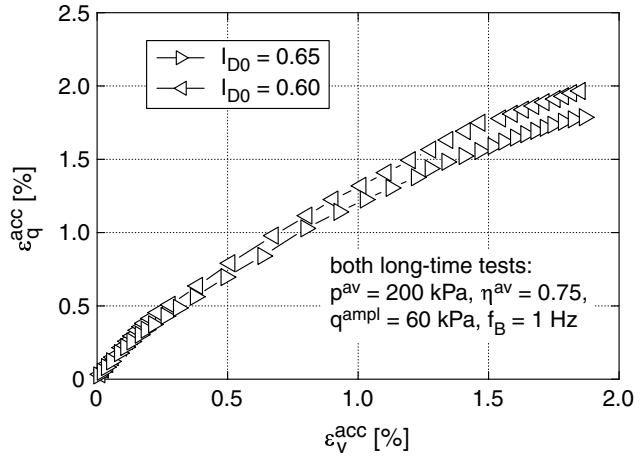

Figure 19: ε_q^{acc}-ε_v^{acc}-*strain paths in two tests with* $N_{\max} = 2 \cdot 10^6$ *cycles*

5.7 Influence of a static (monotonic) preloading

Also the influence of a monotonic preloading on **m** was tested. The specimens were loaded radially along the p-axis or along a K_0-line (with an inclination $\eta = 0.75$) up to a certain preloading pressure 100, 200 or 300 kPa, Fig. 20a. After five minutes the samples were unloaded to $p^{\mathrm{av}} = 100$ kPa. Subsequently, 10^4 cycles with an amplitude $q^{\mathrm{ampl}} = 50$ kPa were applied at $p^{\mathrm{av}} = 100$ kPa and $\eta^{\mathrm{av}} = 0$ or $\eta^{\mathrm{av}} = 0.75$, respectively. The tests with $p_{\mathrm{preload}} = 100$ kPa correspond to a non-preloaded specimen. Figure 20b makes clear, that the ε_q^{acc}-ε_v^{acc}-strain paths of the three tests with the K_0-preloading nearly coincide. A similar conclusion can be drawn for the isotropic preloading. Thus, a monotonic preloading does hardly affect the direction of strain accumulation.

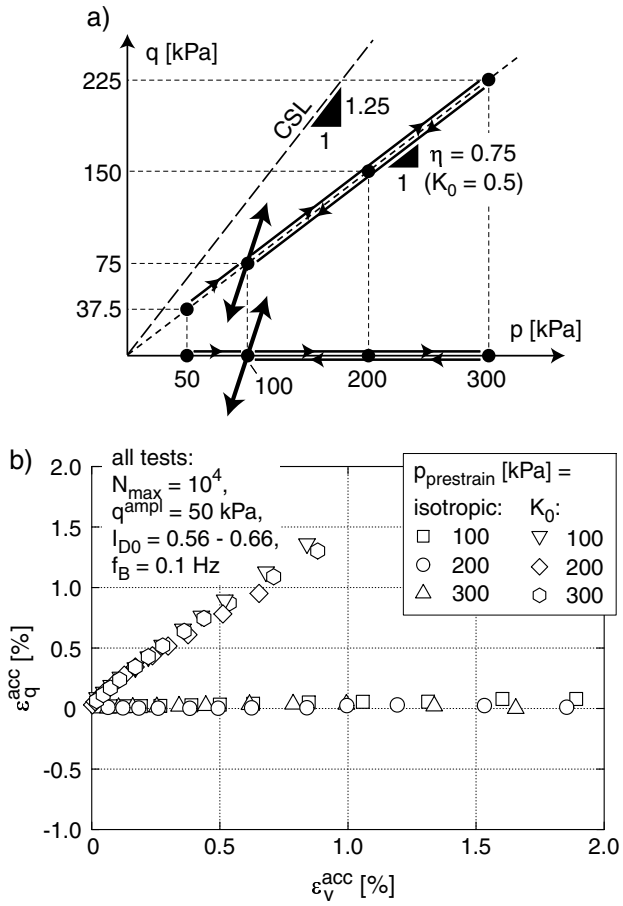

Figure 20: ε_q^{acc}-ε_v^{acc}-*strain paths for a cyclic loading after a monotonic (isotropic or* K_0*) preloading*

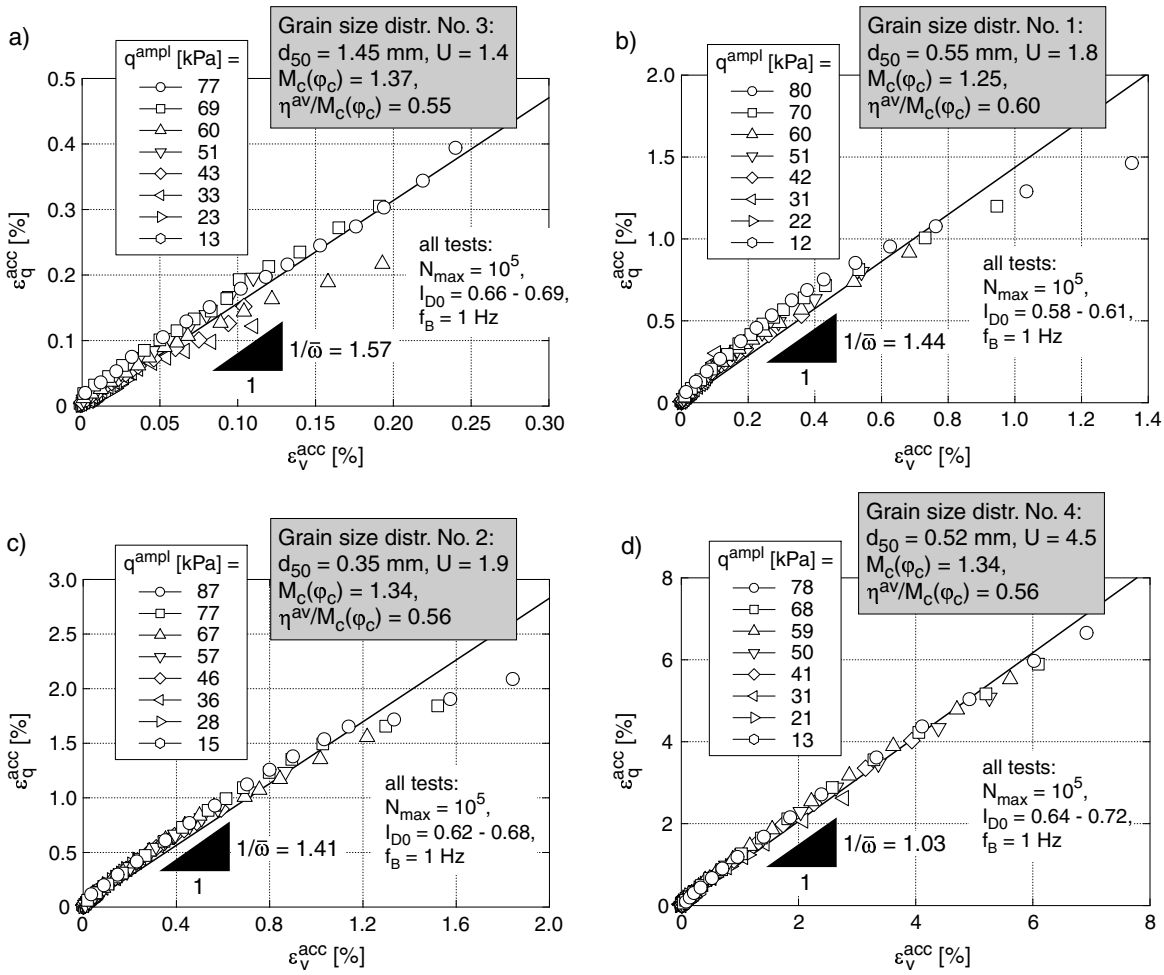

Figure 21: ε_q^{acc}-ε_v^{acc}-*strain paths for different grain size distributions (all tests:* p^{av} *= 200 kPa,* η^{av} *= 0.75)*

5.8 Influence of the grain size distribution curve

All preceding remarks on the cyclic flow rule referred to sand with the grain size distribution curve No. 1 (d_{50} = 0.55 mm, U = 1.8, $\varphi_c = 31.2°$) with respect to Fig. 6. Additionally, the sands with the grain size distribution curves No. 2 (d_{50} = 0.35 mm, U = 1.9, $\varphi_c = 33.3°$), No. 3 (d_{50} = 1.45 mm, U = 1.4, $\varphi_c = 33.9°$) and No. 4 (d_{50} = 0.52 mm, U = 4.5, $\varphi_c = 33.3°$) were tested. In the tests the average stress (p^{av} = 200 kPa, η^{av} = 0.75) was kept constant and the stress amplitude 12 kPa $\leq q^{\mathrm{ampl}} \leq$ 87 kPa was varied.

Figure 21 presents the $\varepsilon_q^{\mathrm{acc}}$-$\varepsilon_v^{\mathrm{acc}}$-strain paths for the sands Nos. 1 to 4. The diagram 21b for sand No. 1 repeats Fig. 13a in order to facilitate comparison. Despite some scatter in the tests on sand No. 3, also for the three sands tested additionally the cyclic flow rule does hardly depend on the stress or strain amplitude. The mean inclination of the strain paths in the $\varepsilon_q^{\mathrm{acc}}$-$\varepsilon_v^{\mathrm{acc}}$-diagram of the medium coarse sand No. 2 ($1/\bar{\omega} = 1.41$) is slightly smaller than the one for the medium coarse to coarse sand No. 1 ($1/\bar{\omega} = 1.44$). For the coarse sand No. 3, **m** is more deviatoric ($1/\bar{\omega} = 1.57$), for the well-graded soil No. 4 it is more compactive ($1/\bar{\omega} = 1.03$). However, these differences may be contributed to the different accumulation rates and the resulting different residual strains. The larger the residual strains are, the smaller is the mean inclination $1/\bar{\omega}$. This becomes evident, if the $\varepsilon_q^{\mathrm{acc}}$-$\varepsilon_v^{\mathrm{acc}}$-strain paths of the four tested sands are presented in a common diagram for $\varepsilon_v^{\mathrm{acc}} \leq 2\%$ (Fig. 22). The difference in the strain paths in Fig. 22 is relatively small. Thus, it can be concluded that the direction of strain accumulation does not significantly depend on the grain size distribution curve.

6 Summary and conclusions

Numerous drained cyclic triaxial tests with many ($10^4 \leq N \leq 10^6$) small ($\varepsilon^{\mathrm{ampl}} \leq 10^{-3}$) cycles demonstrate a unique flow rule **m** for non-cohesive soils under

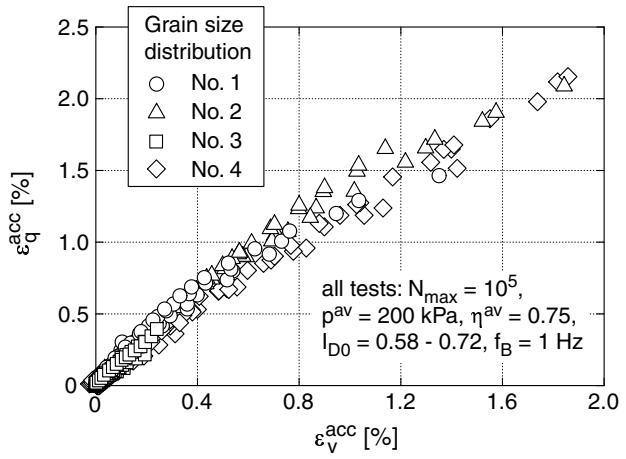

Figure 22: *Summary of the ε_q^{acc}-ε_v^{acc}-strain paths of the four tested grain size distributions for $\varepsilon_v^{acc} \leq 2\%$ in a common diagram*

cyclic loading. The observed flow rule depends mainly on the average stress ratio $\eta^{\mathrm{av}} = q^{\mathrm{av}}/p^{\mathrm{av}}$. A slight increase of the compactive portion with the accumulated strain $\varepsilon^{\mathrm{acc}}$ (due to the previous cycles) was measured. For $\eta^{\mathrm{av}} =$ constant, the ratio $\dot{\varepsilon}_v^{\mathrm{acc}}/\dot{\varepsilon}_q^{\mathrm{acc}}$ does hardly depend on the average mean pressure p^{av}. In the case of *in-phase* cycles the influence of the amplitude is small. The direction of the cycles in the stress or strain space has some influence on $\dot{\varepsilon}_v^{\mathrm{acc}}/\dot{\varepsilon}_q^{\mathrm{acc}}$, but no simple dependence could be found. For *out-of-phase* cycles (e.g. elliptic stress paths in the p-q-plane), the dependence of $\dot{\varepsilon}_v^{\mathrm{acc}}/\dot{\varepsilon}_q^{\mathrm{acc}}$ on the shape of the stress or strain loop may be neglected in explicit models. Furthermore, the cyclic flow rule is only slightly affected by the void ratio, the loading frequency, the static preloading and the grain size distribution curve. The flow rule under cyclic loading can be well approximated by flow rules for monotonic loading (e.g. by the flow rules of the modified Cam clay model or the hypoplastic model). The flow rule **m** should become a well established concept in explicit modelling of accumulation due to small cycles.

Acknowledgements

This study was conducted as a part of the project A8 "Influence of the fabric change in soil on the lifetime of structures", supported by the German Research Council (DFG) within the Collaborate Research Centre SFB 398 "Lifetime oriented design concepts". The authors are indepted to DFG for this financial support.

References

[1] G. Bouckovalas, R.V. Whitman, and W.A. Marr. Permanent displacement of sand with cyclic loading. *Journal of Geotechnical Engineering, ASCE*, 110(11):1606–1623, 1984.

[2] C.S. Chang and R.V. Whitman. Drained permanent deformation of sand due to cyclic loading. *Journal of Geotechnical Engineering, ASCE*, 114(10):1164–1180, 1988.

[3] V.A. Diyaljee and G.P. Raymond. Repetitive load deformation of cohesionless soil. *Journal of the Geotechnical Engineering Division, ASCE*, 108(GT10):1215–1229, 1982.

[4] A. Gotschol. Veränderlich elastisches und plastisches Verhalten nichtbindiger Böden und Schotter unter zyklisch-dynamischer Beanspruchung. Dissertation, Universität Gh Kassel, 2002.

[5] G. Gudehus. A comprehensive constitutive equation for granular materials. *Soils and Foundations*, 36:1–12, 1996.

[6] U. Güttler. Beurteilung des Steifigkeits- und Nachverdichtungsverhaltens von ungebundenen Mineralstoffen. Schriftenreihe des Instituts für Grundbau, Wasserwesen und Verkehrswesen, Heft 8, 1984.

[7] W.S. Kaggwa, J.R. Booker, and J.P. Carter. Residual strains in calcareous sand due to irregular cyclic loading. *Journal of Geotechnical Engineering, ASCE*, 117(2):201–218, 1991.

[8] D. Kolymbas. An outline of hypoplasticity. *Archive of Applied Mechanics*, 61:143–151, 1991.

[9] M.P. Luong. Mechanical aspects and thermal effects of cohesionless soils under cyclic and transient loading. In *Proc. IUTAM Conf. on Deformation and Failure of Granular materials, Delft*, pages 239–246, 1982.

[10] W.A. Marr and J.T. Christian. Permanent displacements due to cyclic wave loading. *Journal of the Geotechnical Engineering Division, ASCE*, 107(GT8):1129–1149, 1981.

[11] Z. Mróz, V.A. Norris, and O.C. Zienkiewicz. An anisotropic hardening model for soils and its application to cyclic loading. *International Journal For Numerical And Analytical Methods in Geomechanics*, 2:203–221, 1978.

[12] A. Niemunis. Akkumulation der Verformung infolge zyklischer Belastung - numerische Strategien. In *Beiträge zum Workshop: Boden*

unter fast zyklischer Belastung: Erfahrungen und Forschungsergebnisse, Veröffentlichungen des Institutes für Grundbau und Bodenmechanik, Ruhr-Universität Bochum, Heft Nr. 32, pages 1–20, 2000.

[13] A. Niemunis. Extended hypoplastic models for soils. Habilitation, Veröffentlichungen des Institutes für Grundbau und Bodenmechanik, Ruhr-Universität Bochum, Heft Nr. 34, 2003. available from `www.pg.gda.pl/~aniem/an-liter.html`.

[14] A. Niemunis and I. Herle. Hypoplastic model for cohesionless soils with elastic strain range. *Mechanics of Cohesive-Frictional Materials*, 2:279–299, 1997.

[15] A. Niemunis, T. Wichtmann, and T. Triantafyllidis. A high-cycle accumulation model for sand. *Computers and Geotechnics*, 32(4):245–263, 2005.

[16] A. Sawicki and W. Świdziński. Compaction curve as one of basic characteristics of granular soils. In E. Flavigny and D. Cordary, editors, *4th Colloque Franco-Polonais de Mechanique des Sols Appliquee*, volume 1, pages 103–115, 1987. Grenoble.

[17] A. Sawicki and W. Świdziński. Mechanics of a sandy subsoil subjected to cyclic loadings. *International Journal For Numerical And Analytical Methods in Geomechanics*, 13:511–529, 1989.

[18] A.S.J. Suiker and R. de Borst. A numerical model for the cyclic deterioration of railway tracks. *International Journal of Numerical Methods in Engineering*, 57:441–470, 2003.

[19] A.S.J. Suiker, E.T. Selig, and R. Frenkel. Static and cyclic triaxial testing of ballast and subballast. *Journal of Geotechnical and Geoenvironmental Engineering, ASCE*, 131(6):771–782, 2005.

[20] K.C. Valanis and C.F. Lee. Endochronic theory of cyclic plasticity with applications. *Journal of Applied Mechanics*, 51:367–374, 1984.

[21] P.-A. von Wolffersdorff. A hypoplastic relation for granular materials with a predefined limit state surface. *Mechanics of Cohesive-Frictional Materials*, 1:251–271, 1996.

[22] P.-A. von Wolffersdorff and R. Schwab. Schleuse Uelzen I - Hypoplastische Finite-Elemente-Analyse von zyklischen Vorgängen. *Bautechnik*, 78(11):771–782, 2001.

[23] T. Wichtmann. Explicit accumulation model for non-cohesive soils under cyclic loading. Dissertation, Schriftenreihe des Institutes für Grundbau und Bodenmechanik der Ruhr-Universität Bochum, Heft 38, 2005.